Bull. Mater. Sci., Vol. 39, No. 6, October 2016, pp. 1593–1601. © Indian Academy of Sciences.
DOI 10.1007/s12034-016-1287-7

Electromagnetic properties of nanocrystalline Al^{3+} substituted MgCuMn ferrites synthesized by microwave hydrothermal method

T RAMESH[1,*] and S R MURTHY[2]
[1]Department of Physics, BVRIT Hyderabad College of Engineering for Women, Hyderabad 500 090, India
[2]Department of Physics, Osmania University, Hyderabad 500 007, India

MS received 12 October 2015; accepted 21 March 2016

Abstract. **The effect of Al^{3+} substitution on electromagnetic properties has been studied for nanocrystalline $Mg_{0.8}Cu_{0.2}Mn_{0.05}Al_xFe_{1.95-x}O_4$ ferrites, wherein x varies from 0 to 0.4 in steps of 0.1. These ferrites were synthesized by using microwave hydrothermal method and then characterized using X-ray diffractometer (XRD), Fourier transform infrared and transmission electron microscopy. The synthesized powders were densified using microwave sintering method at 950°C/50 min. Structural and surface morphology of sintered samples were characterized using XRD and atomic force microscopy, respectively. The complex permittivity and permeability properties were measured over a frequency range 100 Hz–1.8 GHz. The temperature variation of magnetic properties were measured in the temperature range of 300–650 K. The electrical and magnetization studies inferred that the values of d.c. resistivity increases by 27%, whereas saturation magnetization decreases linearly from 38.6 to 23.0 emu g^{-1} and Curie temperature was found to be decreased from 628 to 513 K with an increase of Al^{3+} ions. The low dielectric, magnetic losses, moderate saturation magnetization and high-temperature stability properties exhibited by Al^{3+} substituted MgCuMn ferrites make them find applications in microwave devices, such as circulators and isolators etc. The applicability of present samples for microwave devices has been tested by the measurement of ferromagnetic resonance linewidth at K_a band.**

Keywords. **Ferrite; microwave hydrothermal; magnetic properties; FMR linewidth.**

1. Introduction

Spinel ferrites have received special attention by researchers in recent years as important magnetic compounds of vital technological interest due to their useful applications. These materials are successfully used in different fields like in high-frequency devices [1], microwave devices [2], photocatalysis [3], gas sensors [4], drug delivery [5] and hyperthermia [6]. The general formula for spinel ferrites is AB_2O_4, where A is a divalent metal ion (e.g., magnesium, zinc, nickel and cobalt) and B usually iron substituted sometimes with other trivalent metal ions (e.g., Cr, Al and rare earths). The properties of these compounds are dependent on the distribution of cations between tetrahedral (A) and octahedral (B) sites.

In the present investigation, magnesium-copper-manganese ferrites were selected as a spinel of choice because of its recognized technological applications in nonreciprocal microwave devices like circulators and isolators. In such materials, magnetic and dielectric losses can be minimized by reducing porosity and keeping resistivity high. Compositional tailoring of the magnesium ferrites has been very critical in achieving desirable magnetic and dielectric performance, particularly focusing on the substitution of tetrahedral (A) or octahedral (B) site in the ferrite structure with appropriate chemical elements. Previous studies showed that the minute substitutions of cations like divalent Cu^{2+} and trivalent Mn^{3+} can improve electrical resistivity and density properties of ferrites [7,8]. Recently, it has been reported that the magnetic properties are modified and show interesting behaviour when Al^{3+} (diamagnetic: $\mu_B = 0$) ions are substituted for Fe^{3+} (magnetic; 5 μ_B ions) in ferrites [9]. In general, the properties of ferrites are sensitive to their composition and microstructures, which in turn depend upon the method used for synthesizing them. The most common synthesis technique for ferrite-type materials is the classical ceramic method, but this technique has some inherent disadvantages such as chemical inhomogeneity and introduction of impurities during ball milling. Therefore, the wet chemical techniques such as sol–gel, co-precipitation, hydrothermal, microemulsion and microwave hydrothermal (M–H) are more often employed for such purposes. Out of all the methods, M–H synthesis [10,11] is found to be well suited for obtaining ferrite nanopowders with finite size and shape. Therefore, in the present investigation Al^{3+} substituted MgCuMn ferrite nanopowders were synthesized using M–H method. The synthesized powders were characterized using X-ray diffractometer (XRD), Fourier transform infrared (FTIR) and transmission electron microscopy (TEM), and then sintered using microwave sintering method [12]. A detailed study on the effect of Al^{3+} substitution on electromagnetic properties has been the focus of this study. The applicability of presently investigated ferrites for

*Author for correspondence (rameshouphysics@gmail.com)

microwave devices has been tested by the measurement of ferromagnetic resonance (FMR) linewidth at K_a band.

2. Experimental

The nanopowders of MgCuMnAl ferrites were synthesized starting with pure (Sigma, 99.8%) chemicals of magnesium nitrate [$Mg(NO_3)_2{\cdot}6H_2O$], copper nitrate [$Cu(NO_3)_2{\cdot}6H_2O$], aluminium nitrate [$Al(NO_3)_3{\cdot}9H_2O$], manganese nitrate [$Mn(NO_3)_3{\cdot}9H_2O$] and ferric nitrate [$Fe(NO_3)_3{\cdot}9H_2O$]. The molar ratio of metal nitrates was stoichiometrically adjusted in such a way to obtain the composition $Mg_{0.8}Cu_{0.2}Mn_{0.05}Al_xFe_{1.95-x}O_4$ (where $x = 0.0$ (MH0), 0.1 (MH1), 0.2 (MH2), 0.3 (MH3) and 0.4 (MH4)) and then dissolved in deionized water. Later, aqueous KOH (4M) solution was added dropwise to the nitrate solution with stirring at room temperature until the desired pH (∼10) value was attained. Then the solution was transferred into a Teflon-lined autoclave and treated at a selected temperature (i.e., 150°C) for a specific time (40 min) using a microwave digestion system (model MDS-2000, CEM Corp., Mathews, NC). This system uses 2.45 GHz microwaves and can operate at 0–100% full power (630 ± 50 W). The products obtained after the microwave reaction were filtered and washed repeatedly with deionized water and absolute ethyl alcohol followed by drying overnight at 80°C. Then the synthesized powder was weighed; the percentage yield was calculated and found to be in the range 94–96%.

The synthesized powders were characterized using XRD (Philips PW-1730) with Cu-K_α radiation ($\lambda = 1.5406$ Å), TEM (model JEM-2010, JEOL) and FTIR (Brucker tensor 27). The as-prepared nanopowders were granulated using 2 wt% polyvinyl alcohol as a binder and then pressed uniaxially at a pressure of 150 MPa to form pellets (8 mm diameter, 3 mm height) and toroidal (5 mm inner diameter, 9 mm outer diameter) specimens. After the binder was burnt out at 300°C, the compacts were microwave sintered at 950°C/50 min. The microwave sintering process was carried out using a specially designed applicator, which consists of a domestic microwave oven having an output power level tunable up to a maximum of 800 W and operating frequency of 2.45 GHz. The sintering temperature was measured using a pt-13% pt-Rh thermocouple with an accuracy of ± 1°C. The structural characterization and surface morphology of the sintered samples were studied by XRD and atomic force microscopy (AFM, Park Systems XE-70), respectively.

The complex permittivity and permeability properties were measured over a wide frequency range using Agilent 4291B impedance analyzer. The d.c. electrical resistivity ($\rho_{d.c.}$) was measured using two-probe method at room temperature. Magnetic properties such as saturation magnetization (M_s) and coercivity (H_c) have been measured from recorded hysteresis loops using vibrating sample magnetometer (Lake Shore: model: 7404). The FMR measurements were carried out using a shorted waveguide method. The external magnetic field was swept at a fixed frequency using a TE_{10} mode propagation in a K_a-band (26.5–40 GHz) waveguide. The microwave magnetic field h_{rf} was applied in the plane of the ferrite thin disk, which is always normal to an external field.

3. Results and discussions

Figure 1 shows the XRD patterns for as-synthesized powders of MgCuMnAl ferrites (MH0–MH4). It can be seen from the figure that the presence of the standard characteristic lattice planes (220), (311), (400), (422), (333) and (440) in the XRD patterns confirms the formation of spinel cubic structure with the Fd3m space group. This is in conformity with the powder diffraction file of JCPDS (88-1943). The absence of additional peaks related to any secondary phase in the XRD patterns ensures the phase purity of the synthesized samples. The average crystallite size of the synthesized powders was calculated from the full-width half-maximum (FWHM) of

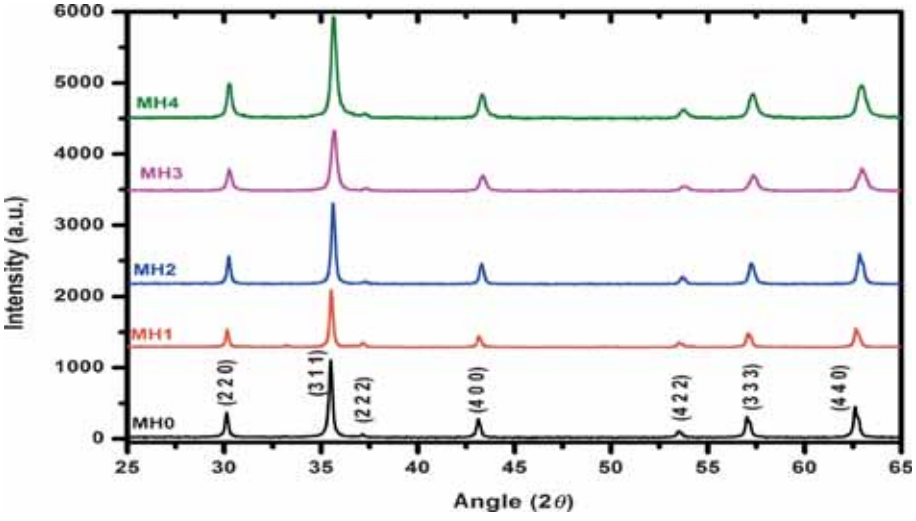

Figure 1. XRD patterns for as-synthesized $Mg_{0.8}Cu_{0.2}Mn_{0.05}Al_xFe_{1.95-x}O_4$ powders.

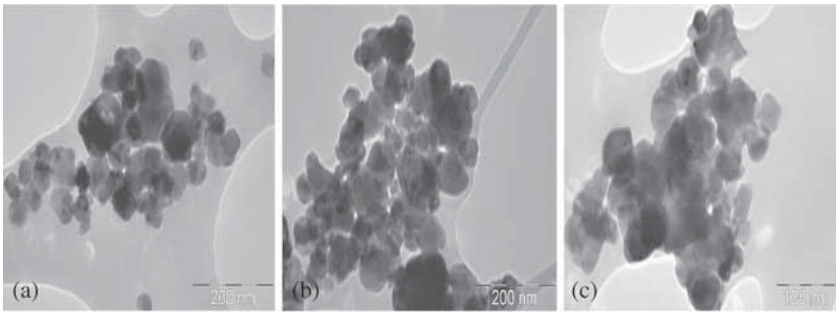

Figure 2. TEM pictures for (**a**) MH0, (**b**) MH2 and (**c**) MH4 ferrite powders.

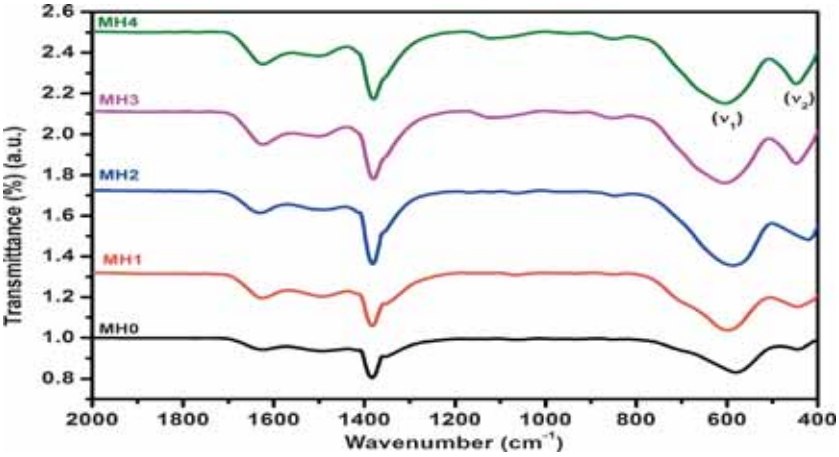

Figure 3. FTIR spectra of all the as-synthesized MgCuMnAl ferrite powders.

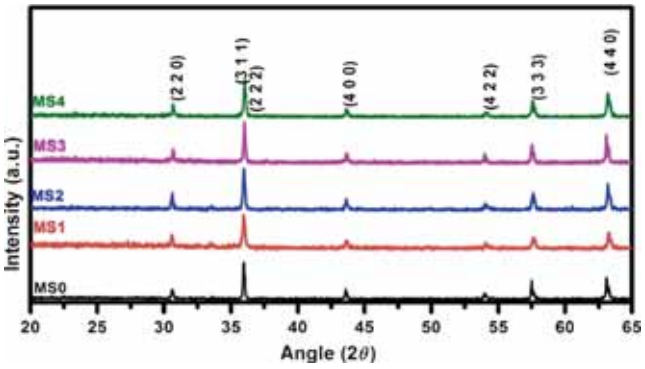

Figure 4. XRD patterns for microwave sintered samples.

the (311) diffraction peak ($2\theta \sim 36°$) by the Scherer formula $D = 0.9\lambda/\beta \cos\theta$, where λ is the wavelength of X-rays used (Cu-K_α = 1.5406 Å), β the FWHM after applying correction due to instrumental broadening and θ represents Bragg's (diffraction) angle. FWHM value for instrumental broadening was carried out initially by running the reference sample (Silicon). This value was then subtracted from the observed value of the sample for the correction. In addition, the values have been checked for other major planes, and they matched with the values reported in this study. The calculated average crystallite sizes of as-synthesized powders are 30, 26, 23, 20 and 16 nm for MH0, MH1, MH2, MH3 and MH4, respectively.

Table 1. Structural properties of $Mg_{0.8}Cu_{0.2}Mn_{0.05}Al_xFe_{1.95-x}O_4$ ferrites.

Sample	Lattice constant (a) (Å)	D_{XRD} (nm)	D_{AFM} (nm)	$d_{X\text{-ray}}$ (g cc^{-1})	P (%)
MS0	8.266	95	102	4.88	5
MS1	8.260	89	95	4.83	5
MS2	8.241	85	89	4.79	6
MS3	8.224	82	86	4.72	7
MS4	8.215	78	81	4.55	8

Figure 2 shows the TEM photograph for three typical as-synthesized ferrite nanopowders. It can be seen from the figures that the nanoparticles were well distributed in the powders without showing any agglomeration. Average particle sizes have been estimated from TEM photographs as 28, 25, 23, 19 and 15 nm for MH0, MH1, MH2, MH3 and MH4 powders, respectively. It can be observed from the above results that the particle size obtained from XRD and TEM measurements were found to be in good agreement with each other.

Figure 3 shows the FTIR spectra for the as-synthesized powders. It can be seen from the figure that a high intensity band has been observed at 1627 cm^{-1}, which represent O–H stretching vibration interacting through H-bonds. Another band ν (C=O) can be seen in the figure at around 1380 cm^{-1}

due to stretching vibration of the carboxylate group (CO_2^{2-}). The absence of any absorption band around 1016 cm^{-1} confirms our powders were free from nitrates. Two more bands were observed in the range of 1000–400 cm^{-1} and they are 550–600 cm^{-1} (ν_1) and 410–450 cm^{-1} (ν_2). The absorption bands ν_1 and ν_2 arise mainly due to the stretching vibrations of the tetrahedral and octahedral metal–oxygen bonds, respectively. The difference in the position of the two strong bonds can be explained based on the differences in the Fe–O bond lengths at A- (1.890–1.879 Å) and B-sites (1.982–1.970 Å).

In the present system, with an increase of Al^{3+} concentration the shift in the higher frequency band, ν_1, is low, whereas in the lower frequency band, ν_2, is more. It suggests that Al^{3+} ions preferentially occupy octahedral sites with a smaller radius and lower atomic weight. The shifting of these bands towards higher frequency side can be attributed to the decrease in the dimensions of the unit cell. Therefore, the decrease in lattice constant with Al^{3+} ion concentration in presently investigated ferrites also confirms the same.

Figure 4 shows the XRD patterns for microwave sintered $Mg_{0.8}Cu_{0.2}Mn_{0.05}Al_xFe_{1.95-x}O_4$ samples (where $x = 0.0$

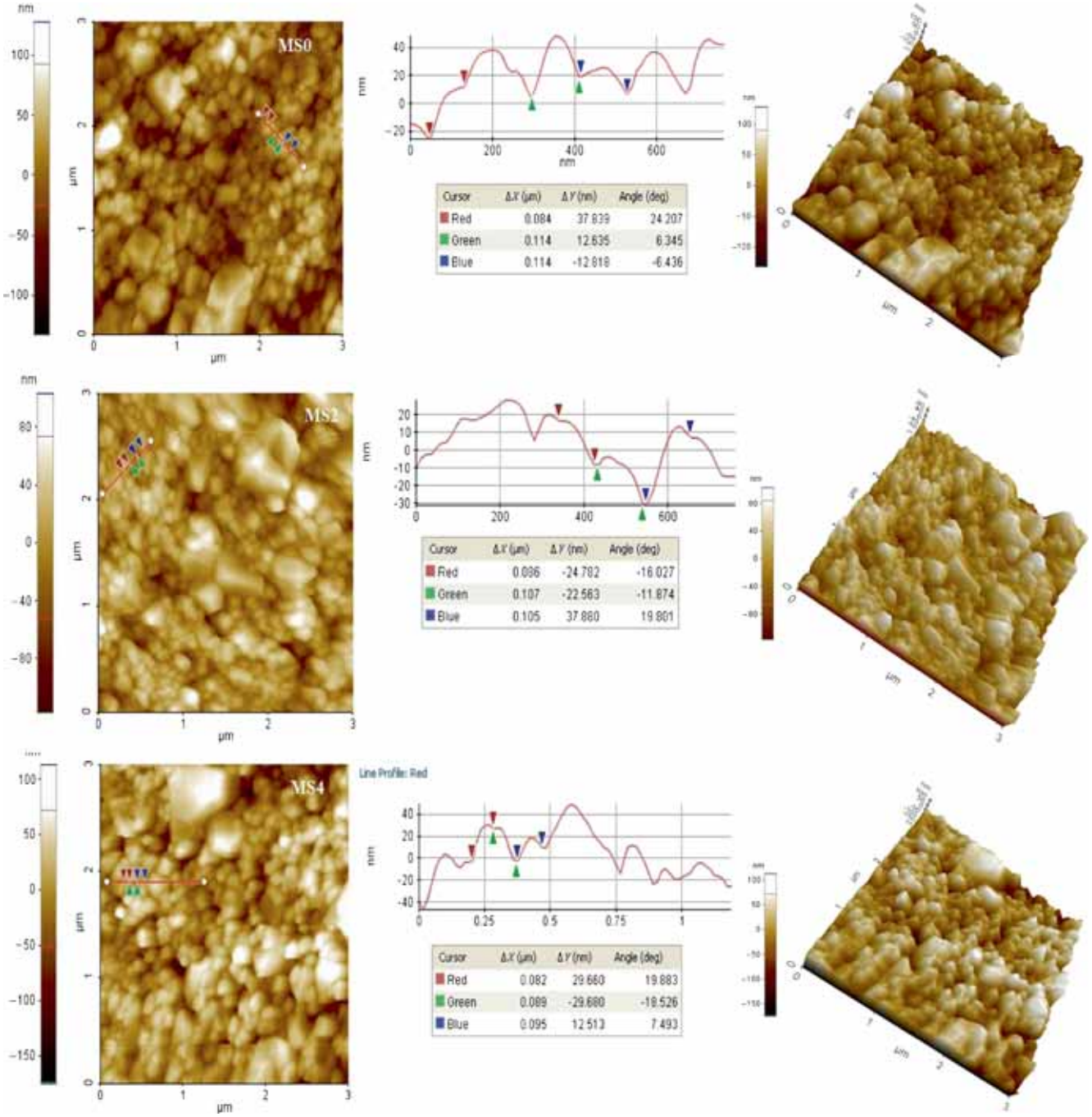

Figure 5. AFM pictures for MS0, MS2 and MS4 samples.

(MS0), 0.1 (MS1), 0.2 (MS2), 0.3 (MS3) and 0.4 (MS4)). It can be seen from the figure that the present samples are monophasic in nature. The grain size (D_m) of the sintered ferrites has been calculated by using Scherer's equation and the results obtained are presented in table 1. The lattice parameter calculated using Nelson–Riley method decreases from 8.266 Å for $x = 0$ to 8.215 Å for $x = 0.4$. This may be attributed to the smaller ionic radius of the Al^{3+} ion (0.515 Å), which has a strong octahedral site preference [13], compared to the substituted Fe^{3+} ionic radius (0.645 Å). The partial replacement of Fe^{3+} ions by Al^{3+} ions will then be expected to cause shrinkage of the unit cell. Furthermore, the higher binding energy and bond strength of Al–O compared to Fe–O [14] cannot be ignored. The obtained values of the lattice parameters exhibited a linear content (Al^{3+} ion) dependence, thus obeying the Vegard's law [15], as given in table 1. The above variation in both the grain size and lattice parameters is in full agreement with the experimental results of most of the previous works [13,14]. The X-ray density ($d_{X\text{-ray}}$) of the ferrite samples (MS0–MS4) has been calculated using the relation $d_{X\text{-ray}} = 8M/Na^3$, where M is the molecular weight of the sample, N the Avogadro number, 8 the number of molecules in the unit cell of spinel lattice and a the lattice constant. The obtained results are presented in table 1. From the table, it can be observed that the X-ray density linearly decreases with the Al^{3+} despite a decrease in the volume of unit cell, suggesting that the rate of decrease in the mass overtakes the rate of decrease in the volume of the unit cell. The bulk densities of the sintered samples were measured using the Archimedes method. The value of bulk densities decreases with the increase of Al^{3+} substitution. However, the present investigated samples possess 92–95% of theoretical density. The high density of the samples is mainly due to the advance kinematics of microwave sintering method than the conventional sintering method. The porosity P (%) percentage of all the samples was calculated using the equation P (%) = {1–(bulk density (d_B)/X-ray density (d_X))}, and the results are presented in table 1. The data reported in the table are an average of at least five readings, and the porosity was found to increase from 5 to 8% in the series.

Figure 5 shows the AFM pictures for three typical (MS0, MS2 and MS4) samples. It can be seen from the figure that the present samples consist of regular grains with a narrow distribution of grain size. Figure 5 also shows the three-dimensional grain size distribution of the present samples. The present microwave sintered samples are composed of nanocrystalline grains with the spherical shape, and the grain size of the samples are in the range of 81–102 nm and the results are presented in table 1. It can be seen from the table that the grain size decreases slightly with an increase of Al^{3+} concentration. The present investigated samples show high densities and, most importantly, a fully homogeneous microstructure well below a very low sintering temperature. Several researchers observed the similar behaviour in case of different microwave sintered ceramics [16,17], which is mainly due to the advanced kinetics of microwave sintering method than the conventional sintering method.

Figure 6 shows the complex permittivity ($\varepsilon^* = \varepsilon' + i\varepsilon''$) spectra for microwave sintered $Mg_{0.8}Cu_{0.2}Mn_{0.05}Al_xFe_{1.95-x}O_4$ samples at room temperature. It can be seen from the figure that the values of real (ε') and imaginary (ε'') permittivities are high in the low-frequency region, and decrease rapidly with increasing frequency up to 10 kHz and then exhibit almost frequency independent behaviour in the high frequency region. The variation of dielectric constant with frequency can be explained on the basis of dispersion caused by the Maxwell–Wagner interfacial polarization with Koop's phenomenological theory [18]. The higher value of ε' in the lower frequency region is mainly due to the electron hopping between Fe^{3+} and Fe^{2+} of octahedral sites. The electrons reach the grain boundary through hopping and are piled up at the grain boundaries, and build up a potential barrier. This accumulation of charge at the grain boundary results in the interfacial polarization. However, as the frequency is increased, the probability of electrons reaching the grain boundary decreases, which results in a decrease in the interfacial polarization. Therefore, the real permittivity decreases with increasing frequency and almost the frequency independent behaviour of ε' is observed within the frequency range of 100 kHz to 600 MHz. With further increase of frequency, the value of ε' is found to increase and shows a resonance peak at 1.2 GHz.

The imaginary part (ε'') of permittivity results due to the lag in polarization vis-a-vis the varying electric field. If the electric polarizations are independent of the varying electric field, loss in the charge storing capacity of materials occurs. In general, the polarization lags behind when the field increases due to the presence of impurities and imperfections in the sample structure, thereby increasing the ε''. Moreover, it can also be seen that the drop in the imaginary part of the permittivity is more pronounced than the real part in the lower frequency region. Imaginary part of permittivity (ε'') for the presently investigated samples is found to be low and remain constant in the wide frequency range of 100 kHz to 600 MHz. The lower value of dielectric loss obtained in the present work can be attributed to the curtailing of the Fe^{2+} ions on account of the hydrothermal process, resulting in better compositional stoichiometry and crystal structure. The resonance peak observed in the ε' and ε'' *vs.* frequency plots around 1.2 GHz arises when the hopping frequency of electrons becomes equal to the applied field frequency, where a maximum electrical energy is transferred to the oscillating ions and power loss shoots up, thereby resulting in resonance. Several researchers [19,20] observed the similar behaviour of ε' and ε'' with frequency for the various ferrite systems. The frequency where the resonance and antiresonance are observed depends on the chemical composition, sintering density etc. The observed ε' and ε'' values of the present investigated samples at 1 MHz are given in table 2. From the table, it can be observed that the values of both ε' and ε'' decrease with an increase in Al^{3+} ion concentration. In general, the addition of Al^{3+} ions in

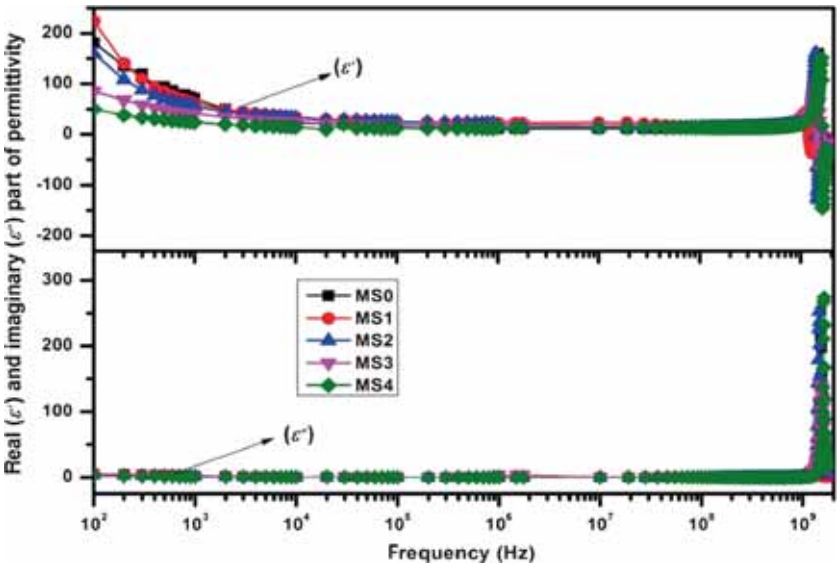

Figure 6. Complex permittivity spectra for microwave sintered $Mg_{0.8}Cu_{0.2}Mn_{0.05}Al_xFe_{1.95-x}O_4$ samples.

Table 2. Electrical and magnetic properties of $Mg_{0.8}Cu_{0.2}Mn_{0.05}Al_xFe_{1.95-x}O_4$ ferrites.

Sample	$\rho_{d.c.} \times 10^7$ (Ω cm^{-1})	ε' at 1 MHz	ε'' at 1 MHz	μ' at 1 MHz	μ'' at 1 MHz	M_S (emu g^{-1})	H_c (Oe)	T_c (K)
MS0	4.6	23	1.10	776	1.70	38.6	69	628
MS1	9.1	20	1.12	685	1.92	33.2	55	603
MS2	52	17	0.96	655	1.19	29.8	40	583
MS3	78	16	0.78	592	1.52	26.4	46	559
MS4	125	13	0.57	513	1.20	23.0	55	513

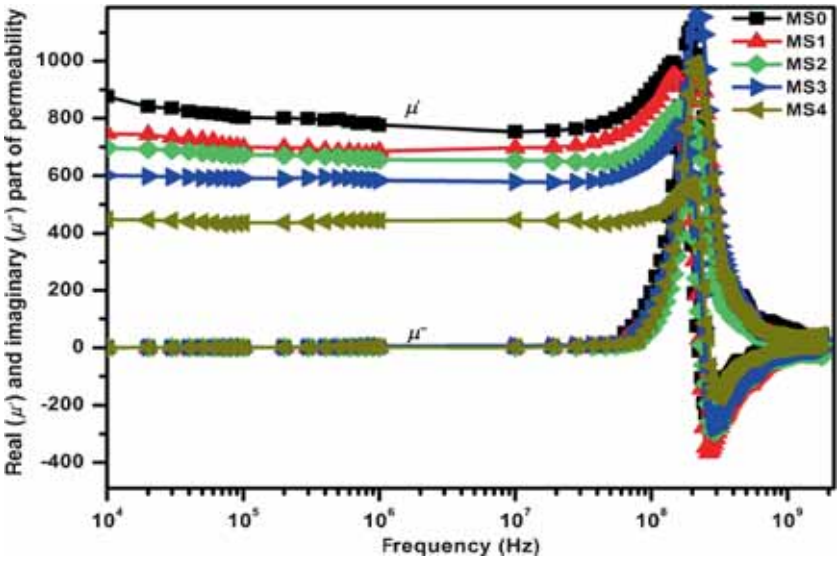

Figure 7. Complex permeability spectra for microwave sintered $Mg_{0.8}Cu_{0.2}Mn_{0.05}Al_xFe_{1.95-x}O_4$ samples.

the place of Fe^{3+} ions limits the degree of conduction and polarization by blocking Verwey's hopping mechanism, which results in the decrease in dielectric constant. Thus, the present investigated samples possess relatively lower losses. These low loss materials, hence, could be useful up to higher frequencies.

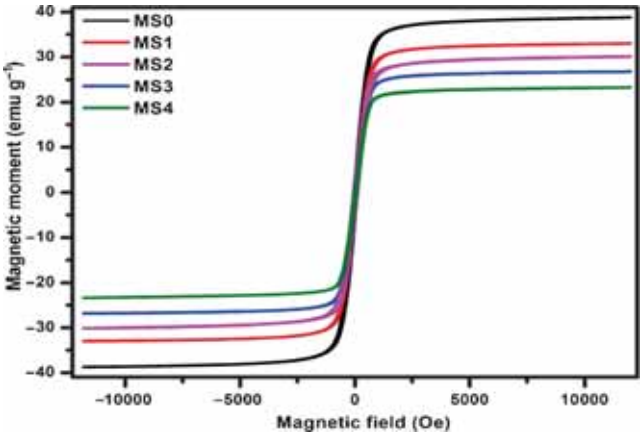

Figure 8. Room-temperature magnetic hysteresis loops for microwave sintered $Mg_{0.8}Cu_{0.2}Mn_{0.05}Al_xFe_{1.95-x}O_4$ samples.

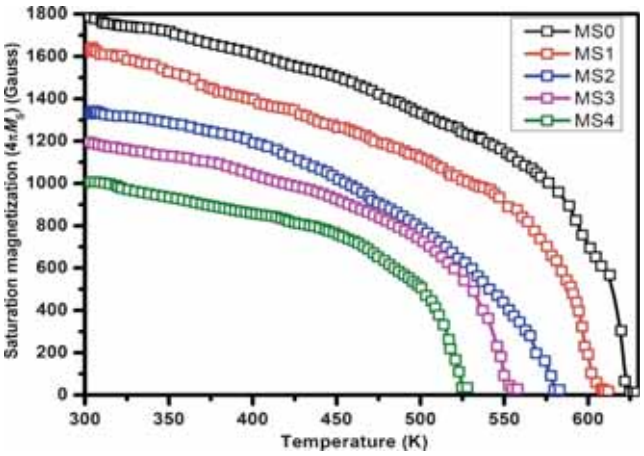

Figure 9. Thermal variation of saturation magnetization ($4\pi M_s$) for microwave sintered $Mg_{0.8}Cu_{0.2}Mn_{0.05}Al_xFe_{1.95-x}O_4$ samples.

In general, the usage of ferrite materials at higher frequencies are limited by eddy current losses and it can be overcome by increasing their d.c. resistivity. Hence, the study of d.c. resistivity is essentiated. In the present investigation, the d.c. resistivity of all the samples has been measured at room temperature by using two-probe method, and the obtained results are presented in table 2. It is evident from the table that the d.c. resistivity increases by two orders with an increase of Al^{3+} substitution to Fe^{3+}. The increase in d.c. resistivity may be due to two facts; firstly, as discussed above that as the Al-concentration increases, the concentration of Fe^{3+} ions decreases and fewer iron ions are available for hopping to take place. Hence, the hopping between Fe^{3+} and Fe^{2+} ions decreases. Secondly, as discussed in the preceding section, the total porosity of the investigated samples increases with increasing Al^{3+} concentration, which in turn hinders the motion of charge carriers, thereby decreasing the mobility of the charge carriers and increasing the resistivity [21].

Figure 7 shows the complex permeability ($\mu^* = \mu' + i\mu''$) spectra for microwave sintered MS0–MS4 samples at room temperature. In general, the complex permeability mainly arises due to two contributions: at low frequencies, wall domain displacements are preponderant and at high frequencies, the spin rotation is the main reason for the permeability [22]. It was observed from the figure that the real (μ') part of permeability remains almost constant until the frequency was raised to a certain value and there onwards at higher frequencies it begins to decrease. The imaginary (μ'') part of permeability gradually increases with the frequency and takes a maximum at a certain frequency, where the μ' rapidly decreases. This feature is well known as natural resonance. As the Al^{3+} concentration increases from 0 to 0.4, the real part of permeability (μ') decreases and the magnetic resonance frequency increases. The compositional variation of real and imaginary part of permeability and magnetic resonance frequency are given in table 2. The table shows that the real (μ') and imaginary (μ'') part of permeability decrease and magnetic resonance frequency increases from 187 to 235 MHz with an increase of Al^{3+} concentration. It can be explained that the change of saturation magnetization in Al^{3+} substituted MgCuMn ferrite is basic ground for change in permeability.

Figure 8 shows the room temperature magnetic hysteresis (M–H) loops for MS0–MS4 samples. The figures reveal that the magnetization increases with increase in the applied magnetic field and attains saturation value at ∼0.2 T. The narrow loops indicate the soft magnetic nature of the present samples. The variation in saturation magnetization (M_s) and coercive field (H_c) with Al^{3+} substitution has been calculated from the M–H loops and obtained results are given in table 2. The table makes it clear that saturation magnetization, remanent magnetization and coercivity decrease with increase in Al^{3+} substitution. In the present investigated $Mg_{0.8}Cu_{0.2}Mn_{0.05}Al_xFe_{1.95-x}O_4$ system, the substitution of Fe^{3+} of magnetic moment 5 μ_B by diamagnetic Al^{3+} of magnetic moment μ_B, which has a stronger preference for occupying the octahedral (B) sites, reduces the magnetic moment of the B-sites. Consequently, the net magnetization also decreases through weakening the A–B interactions, which in turn decreases the resultant saturation magnetization. It is also observed from the table that the value of H_c decreases up to $x = 0.2$ and increases for the higher concentration of Al^{3+}. This behaviour could be explained through Brown's relation [23], which is given by $H_c = 2K_1/\mu_0 M_S$, where K_1 is the anisotropy constant, μ_0 the permeability of free space and M_s the saturation magnetization. It is known that the anisotropy field in ferrites results mainly from the presence of Fe^{2+} ions. For $x < 0.2$, M_s decreases and K_1 increases, whereas for $x > 0.2$ both K_1 and M_s decrease with increasing Al^{3+} concentration. Therefore, the increase in H_c is observed for high Al^{3+} concentration.

Figure 9 presents the thermal variation of saturation magnetization (M_s) for MS0–MS4 samples. The figure leads to draw the fact that magnetization decreases with increase in the temperature. This is a typical behaviour of ferrimagnetic materials and can be reasonably attributed to the decrease in thermal energy. It is also observed from the figure that

the temperature stability of magnetization increases with an increase of Al^{3+} content. The Curie temperature values obtained from M_s *vs.* temperature curves are given in table 2. It shows that the value of T_c decreases with the substitution of Al^{3+}. This can be explained on the basis of the number of magnetic ions present in the two sub-lattices and their mutual interactions. As Fe^{3+} ions (magnetic moment = 5 μ_B) are gradually replaced by Al^{3+} ions (magnetic moment = 0 μ_B), the number of magnetic ions begin to decrease at both sites. This weakens the strength of A–B exchange interactions of the type Fe_A^{3+}-O_2-Fe_B^{3+}. Thus, the thermal energy required to offset the spin alignment decreases, thereby decreasing the Curie temperature.

From the above studies, it is found that the samples MS2 and MS3 posses the moderate electrical and magnetic properties with high temperature stability and low magnetic, dielectric losses which are more general requirements for microwave device applications like isolator and circulators. Hence, these samples have been selected for further studies.

FMR measurements at K_a band were performed with an external static field (H_o) applied perpendicular to the sample plane of MS2 and MS3. Figure 10a displays the FMR frequency as a function of the external magnetic field (H_o), and subsequently, the g-factor was extracted to be 2.02 ± 0.04. It can be seen from the figure that the resonance frequency decreases with increase in external field in both the samples. This is related to an unsaturated magnetizing process in which the external field that is not beyond 16 kOe, which is less than the anisotropy field H_a = 17 kOe for both the samples.

Figure 10b shows the frequency dependence of ferromagnetic resonance linewidths for MS2 and MS3 samples at K_a frequency band (26.50–40 GHz). It can be observed from the figure that a broad distribution of FMR linewidth exists in

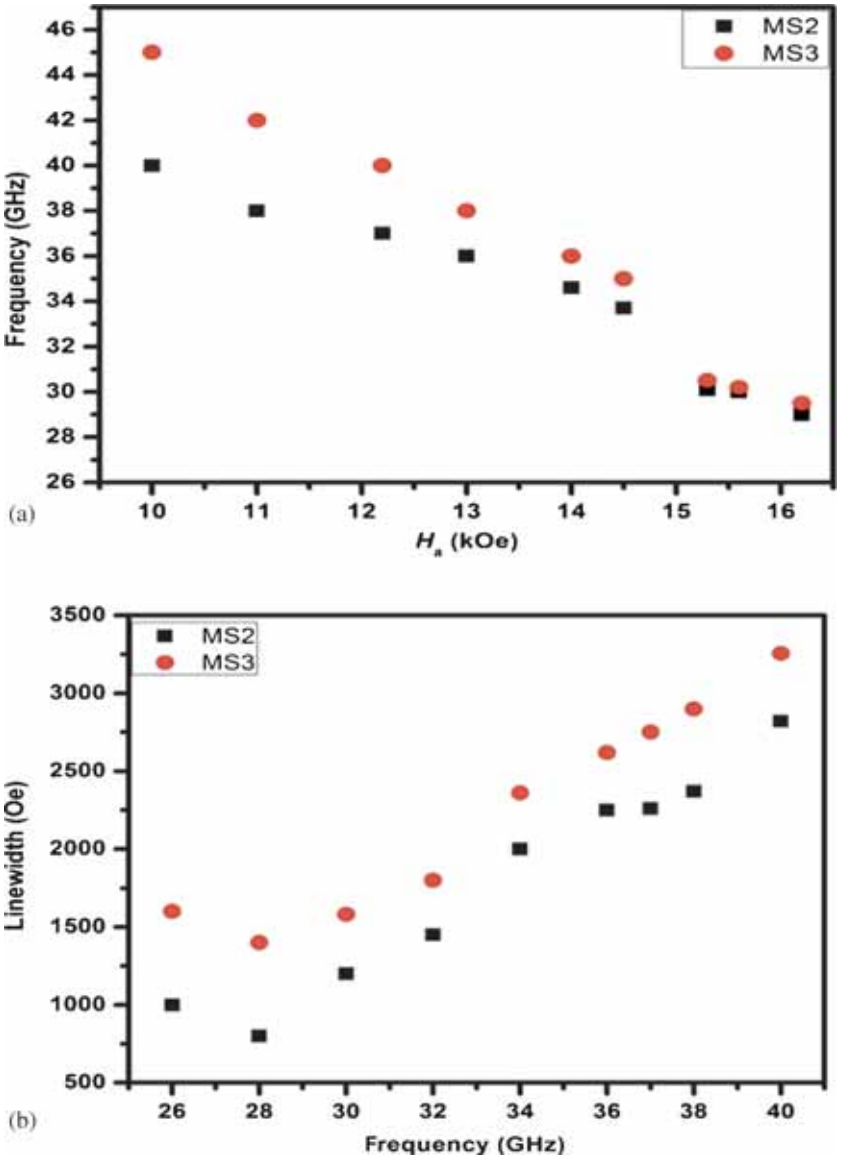

Figure 10. Plots of frequency dependence on (**a**) anisotropy field (H_a) and (**b**) linewidth of MS2 and MS3 samples.

the region where ΔH ranges from 850 to 2000 Oe for MS2 and 1150 to 2210 Oe for MS3 samples. The linewidth gets further broadened with increass in resonance frequency. Mo *et al* [24] observed the similar trend in linewidth in the case of polycrystalline ferrites. Previous studies have indicated that in the case of polycrystalline materials the linewidth majorly depends on the extrinsic contributions, such as porosity, misalignment of anisotropy fields etc., whereas the intrinsic contribution to linewidth is essentially too small to be considered, especially for the randomly oriented polycrystalline materials like our samples. In the present investigation, the MS3 sample shows higher linewidth compared to MS2 at a particular frequency and it may be due to high porosity and the nonmagnetic inclusion of MS3 compared to MS2. However, these results represent the lowest linewidth observed in the present investigated samples compared to our previously studied Ni-based ferrites [25]. This represents around 50% improvement of this critical parameter. This is mainly achieved due to the high density, homogeneity and fine grain size of the present investigated samples. The measured FMR linewidths are believed to have satisfactorily addressed most requirements of microwave devices like circulator and isolator. From all the studies it can be concluded that the presently investigated samples show several salient properties such as high d.c. resistivity, the moderate values of M_s, μ_i and low magnetic, dielectric losses, which are essential properties for the applicability of these materials at higher frequencies. Apart from this, the sample with $x = 0.2$ (MS2) and 0.3 (MS3) possess the high stability of magnetization with low magnetic and dielectric losses. Hence, these properties make them be most commonly used in microwave devices, such as circulators and isolators, particularly at high operating powers and operating frequencies.

4. Conclusions

Nanocrystalline magnesium-manganese-aluminium ferrite powders were synthesized by using microwave hydrothermal method at a low temperature 150°C/40 min. The nanopowders were densified using microwave sintering at 950°C/50 min. After studying the effect of Al^{3+} concentration on the physical, electrical, magnetic and dielectric properties of MgCuMn ferrites, the following conclusions could have been drawn from these results. The d.c. resistivity was observed to increase with increase in Al^{3+} concentration to make these materials suitable for high-frequency applications, wherein less eddy current losses are required. The values of dielectric constant, dielectric loss, initial permeability, saturation magnetization and Curie temperature were found to be decreasing with the increase of Al^{3+} concentration in the place of Fe^{3+}. The low dielectric, magnetic losses combined with an excellent temperature stability of magnetization ($4\pi M_s$) observed in the present ferrites can be utilized in the fabrication of microwave devices, such as circulators, phase shifters etc. The applicability of presently investigated ferrites for microwave devices has been tested by the FMR measurement.

Acknowledgement

Ramesh would like to thank CSIR-New Delhi for providing SRF fellowship to carryout this work.

References

[1] Valenzuela R 2012 *Phys. Res. Int.* **2012** 591839
[2] Harris V G, Geiler, Chen Y, Yoon S D, Wu M, Yang A *et al* 2009 *J. Magn. Magn. Mater.* **321** 2035
[3] Tezuka K, Kogure M and Shan Y J 2014 *Catal. Commun.* **48** 11
[4] Šutka A and Gross K A 2016 *Sens. Actuators B: Chem.* **222** 95
[5] McBain S C, Yiu H H P and Dobson J 2008 *Int. J. Nanomed.* **3** 169
[6] Khot V M, Salunkhe A B, Ruso J M and Pawar S H 2015 *J. Magn. Magn. Mater.* **384** 335
[7] Murthy S R 2001 *Bull. Mater. Sci.* **24** 379
[8] Patil S A, Patil M G, Mahajan V C, Ghatage A K, Lotke S D and Patil R N 1996 *Phase Transitions* **56** 21
[9] Raju K, Balaji C G and Venugopal Reddy P 2014 *J. Magn. Magn. Mater.* **354** 383
[10] Komaraneni S, Roy R and Li Q H 1992 *Mater. Res. Bull.* **27** 1393
[11] Melo R S, Silva F C, Moura K R M, de Menezes A S and Sinfrônio F S M 2015 *J. Magn. Magn. Mater.* **381** 109
[12] Ramesh T, Shinde R S and Murthy S R 2012 *J. Magn. Magn. Mater.* **324** 3668
[13] Ramesh T, Shinde R S and Murthy S R 2013 *J. Magn. Magn. Mater.* **345** 276
[14] Maghsoudi I, Shokrollahi H, Hadianfard M J and Amighian J 2013 *Powder Technol.* **235** 110
[15] Culity B D 1967 *Elements of X-ray diffraction* (Reading Massachusetts: Addison-wesley) 352
[16] Thomazini D, Gelfuso M V, Chinelatto A S A, Chinelatto A L, Sanson F K and Teixeira Neto F 2011 *Ceramica* **57** 45
[17] Madhuri W, Penchal Reddy M, Ramamanohar Reddy N, Siva Kumar K V and Murthy V R K 2009 *J. Phys. D: Appl. Phys.* **42** 165007
[18] Koops C G 1951 *Phys. Rev.* **83** 121
[19] Praveena K, Sadhana K, Bharadwaj S and Murthy S R 2009 *J. Magn. Magn. Mater.* **321** 2433
[20] Ahmad M, Ali I, Grössinger R and Rana M U 2013 *J. Alloys Comp.* **577** 382
[21] Sattar A A, El-sayed H M, El-Shokofy K M and El-Tabey M M 2005 *J. Mater. Sci.* **40** 4873
[22] Tsutaoka T, Ueshima M and Tokunaga T 1995 *J. Appl. Phys.* **78** 3983
[23] Coey J M D. 1996 *Rare earth permanent magnetism*, 1st edn (New York: John Wiley and Sons) p 220
[24] Mo N, Green J J, Krivosik P and Patton C E 2007 *J. Appl. Phys.* **101** 023914
[25] Ramesh T, Shinde R S and Murthy S R 2011 *J. Magn. Magn. Mater.* **323** 1593